Flexible ambipolar organic field-effect transistors with reverse-offset-printed silver electrodes for a complementary inverter

2016 Nanotechnology 27 225302

(http://iopscience.iop.org/0957-4484/27/22/225302)

IOP Publishing Nanotechnology
Nanotechnology 27 (2016) 225302 (11pp) doi:10.1088/0957-4484/27/22/225302

Flexible ambipolar organic field-effect transistors with reverse-offset-printed silver electrodes for a complementary inverter

Junsu Park[1,3], Minseok Kim[1], Seung-Won Yeom[1], Hyeon Jun Ha[1], Hyenggun Song[2], Young Min Jhon[3], Yun-Hi Kim[2,4] and Byeong-Kwon Ju[1,4]

[1] Display and Nanosystem Laboratory, College of Engineering, Korea University, Anam-dong, Seoul 139-713, Korea
[2] Department of Chemistry, Research Institute of Nature Science (RINS), Gyeongsang National University, Jinju 660-701, Korea
[3] Sensor System Research Center, Korea Institute of Science and Technology, Seoul 136-791, Korea

E-mail: ykim@gnu.ac.kr and bkju@korea.ac.kr

Received 22 January 2016, revised 21 March 2016
Accepted for publication 1 April 2016
Published 26 April 2016

Abstract

We report ambipolar organic field-effect transistors and complementary inverter circuits with reverse-offset-printed (ROP) Ag electrodes fabricated on a flexible substrate. A diketopyrrolopyrrole-based co-polymer (PDPP-TAT) was used as the semiconductor and poly (methyl methacrylate) was used as the gate insulator. Considerable improvement is observed in the n-channel electrical characteristics by inserting a cesium carbonate (Cs_2CO_3) as the electron-injection/hole-blocking layer at the interface between the semiconductors and the electrodes. The saturation mobility values are 0.35 $cm^2 V^{-1} s^{-1}$ for the p-channel and 0.027 $cm^2 V^{-1} s^{-1}$ for the n-channel. A complementary inverter is demonstrated based on the ROP process, and it is selectively controlled by the insertion of Cs_2CO_3 onto the n-channel region via thermal evaporation. Moreover, the devices show stable operation during the mechanical bending test using tensile strains ranging from 0.05% to 0.5%. The results confirm that these devices have great potential for use in flexible and inexpensive integrated circuits over a large area.

Keywords: printed electronics, reverse offset printing, ambipolarity, organic semiconductor, field-effect transistors, complementary inverter

(Some figures may appear in colour only in the online journal)

1. Introduction

Recently, organic electronic devices are being used in a broad range of applications such as photovoltaics [1], optical displays [2], memories [3], and sensors [4]. Among the organic electronic devices, organic thin-film transistors and π-conjugated organic semiconductors are especially attractive for large-area, flexible, and low-weight applications. In addition, recent research has resulted in the development of ambipolar organic field-effect transistors (OFETs), which are fabricated using a single semiconductor [5, 6]. They have simpler designs than those based on the p- and n-channel organic semiconductors, because those based on the p- and n-channel materials need a blending of semiconductors or bilayers of semiconductor films [7–10]. Therefore, ambipolar FETs based on a single semiconductor are the easiest to fabricate. However, this method requires superior charge transport for both charge carriers for the field-effect mobility (μ_{FET}) of the transistors. Organic semiconducting co-polymers, which have low bandgaps because of the alternating electron donor–acceptor dyads, have been developed recently for ambipolarity [11–14]. These π-conjugated organic semiconductors based on the donor–acceptor system (the so-called push–pull effect) have favorable charge injections from the electrodes to

[4] Authors to whom any correspondence should be addressed.

their highest occupied molecular orbitals (HOMO) and lowest unoccupied molecular orbitals (LUMO), because of their low bandgaps. Furthermore, a methodology was reported that involves insertion of a thin Cs_2CO_3 layer for controlling the charge injection [15–17]. Through the insertion of Cs_2CO_3 as an electron-injection/hole-blocking layer, the energy levels of the organic semiconductor can be aligned with the work functions of the electrodes for high charge transport performance of both charge carriers. Additionally, by using Cs_2CO_3 as the electron-injection layer, more metals can be used as electrodes, and the devices show higher power efficiencies than those using LiF, which is a well-known electron-injection layer [18]. Moreover, optimized currents can be achieved by adjusting the thickness of the deposited Cs_2CO_3. Therefore, the use of Cs_2CO_3 as the electron-injection layer has increased in the organic electronic devices.

Over the past few years, solution-processable metal electrodes for printed electronic devices have become attractive for their processing methods. Printed electronic-device methods have received more attention than the conventional photolithography processes that requires many fabrication steps, because of their simple and low-cost processes for flexible and large-area applications. Various types of graphic-art printing techniques such as gravure [19], offset [20], inkjet [21], screen [22], flexography [23], and spray [15], have recently been developed for producing a patterned layer. Compared to other printing methods, mass-production printing methods such as gravure, offset printing, and reverse offset printing (ROP) are clearly advantageous for low-cost organic electronic devices using flexible and large-area fabrication techniques. However, mass production roll-to-roll (R2R) processes have limits for the printing resolution and surface morphologies of the printed patterns. Recently, Moon *et al* [24] analyzed a new direct printing method using Ag nanopowder ink for metal electrodes; this was a modified version of the conventional gravure offset printing. First, they coated a soft blanket roll with Ag ink and rolled it onto a glass cliché with electrode patterns. This pickup (off-step) process removes any unnecessary Ag ink outside the electrode pattern. Then, they transferred the remaining Ag ink on the blanket roll to the desired glass substrate (step-step). This method is commonly called ROP. ROP is a mass-production printing method that can achieve high resolution and complicated shape patterns. Previous research on reverse-offset-printed Ag had focused on a single element such as an organic TFTs.

In this study, we investigate ambipolar OFETs and complementary inverters based on reverse-offset-printed Ag nanoparticle electrodes. The OFETs were fabricated on a flexible substrate with a diketopyrrolopyrrole-based co-polymer (PDPP-TAT) as the semiconductor. In addition, by the insertion of Cs_2CO_3 as the charge injection layer at the semiconductor-electrode interface, the LUMO energy level of the semiconductor was aligned with the work function of the electrode because of the change in the energy barrier. A complementary inverter based on reverse-offset-printed Ag electrodes is demonstrated by inserting Cs_2CO_3 onto the n-channel region via thermal evaporation. Finally, the electrical characteristics of the flexible devices were examined for bending radii ranging from 100 to 10 mm.

2. Experiment

2.1. Preparation of reverse-offset-printed Ag electrodes

Ag electrodes were fabricated on a plastic substrate by a roll-to-plate ROP process (Narae Nanotech Co.). Ag nanoparticle paste ink (Ag content: 39 wt%, viscosity: 1.5 cPs, surface tension: 25.8 mN m^{-1}; Advanced Nano Products Co., Ltd) was dispensed on the surface of the PDMS (polydimethylsiloxane) type blanket roll, using a syringe pump. As the blanket was rolled over the cliché, which was patterned using photolithography and reactive ion-etching processes, unnecessary ink was removed from the blanket and transferred to the cliché surface. The Ag ink that remained on the blanket for the desired pattern was transferred onto the plastic substrates. In order to remove the various additives and residual solvents in the printed ink, the substrates were thermally treated at 250 °C on a hotplate for 20 min in air. In addition, the substrates were cleaned using an ultrasonic bath of deionized water, acetone, and isopropyl alcohol, in that order, for 10 min each.

2.2. Field-effect transistor fabrication

Ag electrodes were patterned on the plastic substrates by the ROP process. After the substrates were preheated to 70 °C, Cs_2CO_3 dissolved in 2-ethoxyethanol (2 mg ml^{-1} concentration) was spin-coated at 2000 rpm for 60 s, followed by thermal annealing at 120 °C for 30 min in an Ar-purged glove box. The organic co-polymer semiconductor poly(2,5-bis(2-tetradecyloctadecyl)-3-(thiophen-2-yl)-6-(5′-(thiophen-2-ylethynyl)-2,2′-bithiophen-5-yl)-pyrrolo[3,4-c]pyrrole-1,4 (2H,5H)-dione) (PDPP-TAT) was synthesized, and dissolved in chloroform to obtain a 10 mg ml^{-1} solution. The chloroform solution containing PDPP-TAT, which was preheated to 55 °C, was spin-coated on the substrates at 4000 rpm for 60 s, and then, the substrates were thermally annealed at 150 °C for 10 min in the Ar-purged glove box. PMMA (poly(methyl methacrylate), Sigma Aldrich, $M_w = 120$ k, dielectric constant = 3.5) was used as a dielectric material. PMMA (140 mg ml^{-1} concentration) was dissolved in n-butyl acetate and the solution (preheated to 80 °C) was spin-coated at 2000 rpm for 60 s. The film was then baked at 100 °C for 30 min in the same glove box. The top-gate/bottom-contact structure of the ambipolar FETs was completed by the formation of the gate electrode (Al) by thermal evaporation using a metal shadow mask. The electrical characteristics of the transistor were measured by a Keithley-4200 Semiconductor Parameter Analyzer at room temperature.

2.3. Complementary inverter fabrication

Ag electrodes, which have identical channel lengths of 20 μm and channel widths of 1 mm and 10 mm, were fabricated on the polyimide substrates by the ROP process. The Cs_2CO_3

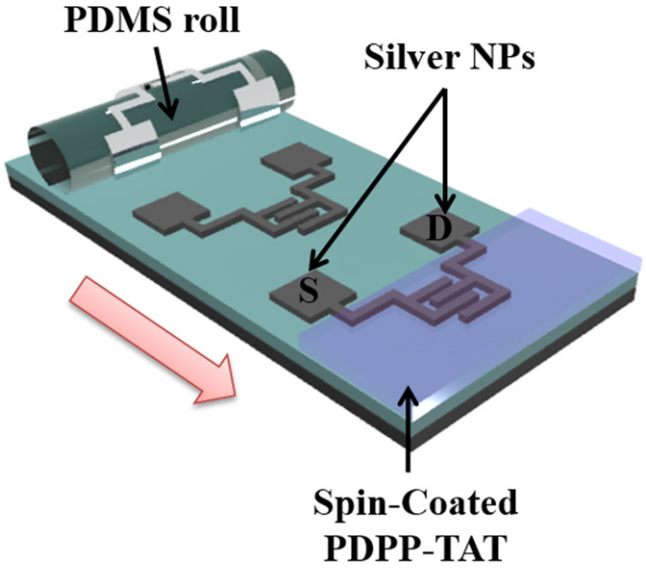

Figure 1. Schematic roll-to-plate ROP process for the fabrication of Ag electrodes.

was deposited on the n-channel transistors of the inverter using thermal evaporation with a shadow mask. PDPP-TAT and PMMA were spin-coated and thermally annealed as the semiconductor layer at 150 °C for 10 min and as the gate dielectric layer at 100 °C for 30 min, respectively. The complementary inverters were completed by the deposition of the Al gate electrodes by using a thermal evaporator with a shadow mask.

2.4. Characterization

The surface states were analyzed using x-ray photoemission spectroscopy (XPS) and ultraviolet photoelectron spectroscopy (UPS) (AXIS-NOVA, Kratos Inc.). The morphologies of the electrodes and semiconductor were characterized using an field emission scanning electron microscope (FESEM, Hitachi S-4300) and Digital Instruments Multimode AFM (atomic force microscopy) under the tapping mode. The electrical characteristics were measured using a Keithley-4200 Semiconductor Parameter Analyzer at room temperature. The fundamental device parameters, such as the saturation mobility (μ_{sat}) and threshold voltage (V_T), were evaluated in the saturation regime using the gradual channel approximation equation.

3. Results and discussion

Figure 1 shows a schematic diagram of the ROP process. Ag electrodes were fabricated on the plastic substrates by a roll-to-plate ROP process (Narae Nanotech Co.). The ambipolar OFETs were fabricated on these flexible substrates and contained four layers (figure 2(a)). Figure 2(b) shows a digital camera image of the flexible ambipolar OFETs, which consist of a 6 × 6 transistor array on a polyimide substrate. The Ag nanoparticle paste was used for fabricating the electrodes with a 20 μm channel length and 1 mm width using a roll-to-plate ROP method at a curing temperature of 250 °C (figure 2(c)). We had previously reported that the conductivity and surface roughness of the Ag nanoparticles cured at 250 °C are optimized on the polyimide substrate, and that the best electrical characteristics of the OFETs with ROP Ag electrodes were observed at the same curing temperature [25]. Au is the most commonly used element for the source/drain electrodes of OFETs, because its work function (5.1 eV for pristine Au) closely matches the HOMO level of the p-channel organic semiconductors [26, 27]. However, Au is expensive, which is a disadvantage for low-cost organic electronics. The work function (Φ) of the ROP electrodes cured at 250 °C was −4.96 eV, as evaluated using UPS, owing to the formation of AgO during thermal annealing [25]. Using ROP-Ag as the electrode is more advantageous for low-cost devices because this value is comparable to the Φ of bare Au. Previously, a comparison of the mobility of the OFETs ROP and evaporated Ag electrodes had been performed [28]. The mobility of ROP-based OFET electrodes was higher than that of evaporated Ag electrodes, because the Ag electrode work function (4.3 eV) is incompatible with the HOMO level of the p-channel organic semiconductors. In addition, the ROP process can produce the pattern more easily when compared with the conventional photolithography and lift-off processes.

A new donor–acceptor co-polymer, PDPP-TAT, was used as the active layer. The PDPP-TAT co-polymers are synthesized by the palladium-catalyzed Stille coupling reaction between 3,6-bis(5-bromothiophen-2-yl)-2,5-bis(2-tetradecyloctadecyl)-pyrrolo[3,4-c]pyrrole-1,4(2H,5H)-dione and 1,2-bis(5-(trimethylstannyl)thiophen-2-yl)ethyne. The number-average molecular weight (M_n) of the synthesized semiconductors is 73.0 kDa with a polydispersity index of 1.31 [29]. Figure 2(d) shows the chemical structure of the organic semiconducting co-polymer, which is based on the push–pull effect. It has a high solubility because of the long alkyl chain. The LUMO and HOMO values of PDPP-TAT measured using the UV–visible absorption spectra from the onset absorptions of the thin films of the semiconductors are 3.89 eV and 5.39 eV, respectively [29]. PMMA, as the gate dielectric layer, was spin-coated and the OFETs of the top-gate /bottom-contact structure were completed by depositing the Al gate electrode using thermal evaporation. This structure has environmental stability because of the auto-encapsulation effect by the gate electrode and the dielectric layer. In addition, the PMMA with hydrophobic end groups ($-CH_3$) can protect the active layer from moisture [30]. PMMA can be dissolved into n-butyl acetate by preheating; whereas, the conjugated polymers do not dissolve in the same solvent [31]. Therefore, PMMA can be deposited on the co-polymers without damaging the surface of the semiconductor layer.

The transfer (drain current I_D versus gate voltage V_G) and output (I_D versus drain voltage V_D) characteristics of the ambipolar FETs using ROP Ag electrodes are shown in figure 3. The fundamental OFET parameters of these devices in the saturation regime ($V_G - V_T < V_D$) are obtained from

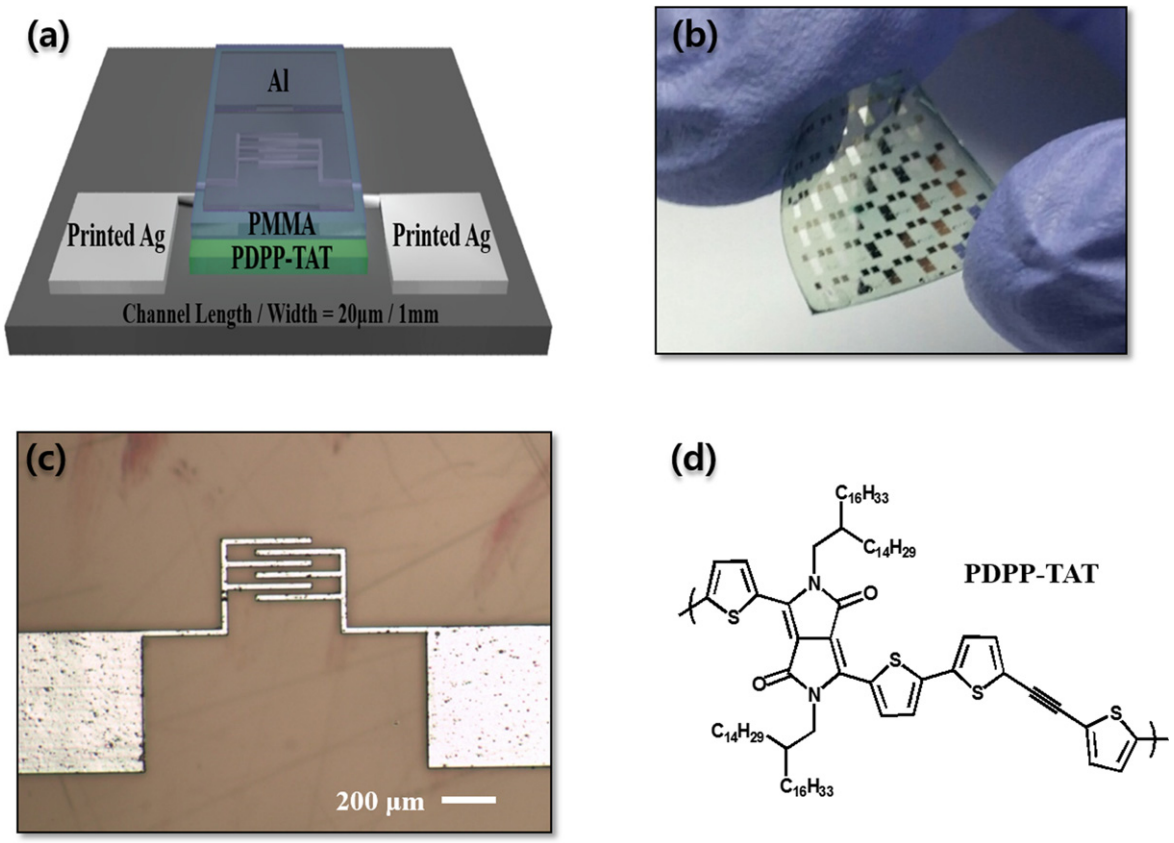

Figure 2. (a) Top-gate/bottom-contact OFET device structure with ROP Ag electrodes. (b) Digital camera image of flexible devices on polyimide substrate. (c) Optical image of ROP Ag electrodes with $W/L = 1000/20\ \mu$m. (d) Chemical structure of the PDPP-TAT organic semiconducting co-polymer.

the following equation:

$$I_D = \frac{W}{2L}\mu_{sat} C_i (V_G - V_T)^2, \quad (1)$$

where, I_D is the source-to-drain current; W and L are the width and length of the channel, respectively; μ_{sat} is the saturation mobility; C_i is the capacitance per unit area of the gate insulator; V_G is the gate voltage; and V_D is the drain voltage. V_T was evaluated from the x-axis intercept of the plot of $\sqrt{I_D}$ versus V_G. The subthreshold swing (SS) is determined from the following equation:

$$S = \frac{dV_G}{d(\log I_D)}. \quad (2)$$

The electrical characteristics of hole-transport are: $\mu_{sat} = 0.35$ (± 0.022) cm^2 V^{-1} s^{-1}, $V_T = -32.3$ (± 2.55) V, SS $= -13.0$ (± 1.89) V decade^{-1}, and $I_{on}/I_{off} \sim 10^4$ at $V_D = 60$ V. In contrast to the operation for the p-channel, the OFETs exhibited poor device performance for n-channel operation with $\mu_{sat} = 0.0084$ ($\pm 0.000\,27$) cm^2 V^{-1} s^{-1}, $V_T = 56.1$ (± 3.01) V, SS $= 27.2$ (± 4.45) V decade^{-1}, and $I_{on}/I_{off} \sim 10^2$ at $V_D = -60$ V (table 1). This is attributed to the energy barrier, at the interface between semiconductors and electrodes, being more favorable for hole injection than for electron.

The n-channel electrical characteristics of ambipolar OFETs can be considerably enhanced by using Cs_2CO_3 as a charge injection layer. Cs_2CO_3, which is soluble in 2-ethoxyethanol, can be spin-coated and deposited by thermal evaporation. As can be observed in figures 4(a) and (b), the transfer and output characteristics of the modified OFETs with the Cs_2CO_3 layer showed greatly improved n-channel electrical characteristics with $\mu_{sat} = 0.027$ (± 0.0015) cm^2 V^{-1} s^{-1}, $V_T = 26.1$ (± 3.15) V, SS $= 12.9$ (± 2.02) V decade^{-1}, and $I_{on}/I_{off} \sim 10^4$ at $V_D = 60$ V. In comparison with the n-channel operation, the hole injection was depreciated and p-channel electrical characteristics were degraded with $\mu_{sat} = 0.26$ (± 0.038) cm^2 V^{-1} s^{-1}, $V_T = -66.3$ (± 4.41) V, SS $= -20.8$ (± 3.27) V decade^{-1}, and $I_{on}/I_{off} \sim 10^2$ at $V_D = -60$ V (figures 4(c) and (d)). However, the modified OFET devices still have outstanding hole transport in spite of the insertion of Cs_2CO_3. As noted previously, this is attributed to the low band gap (1.50 eV) of PDPP-TAT, which has HOMO and LUMO levels of 5.39 eV and 3.89 eV, respectively.

As shown in figure 5(a), we confirmed the component elements on the surface of the Cs-processed ROP Ag using XPS. Figures 5(b) and (c) show that the XPS Ag 3d peak and the XPS O 1s peak are detected at ~368 eV and ~532 eV, respectively. The formation of the Ag oxides which have Fermi levels from −4.8 to −5.1 eV probably resulted from

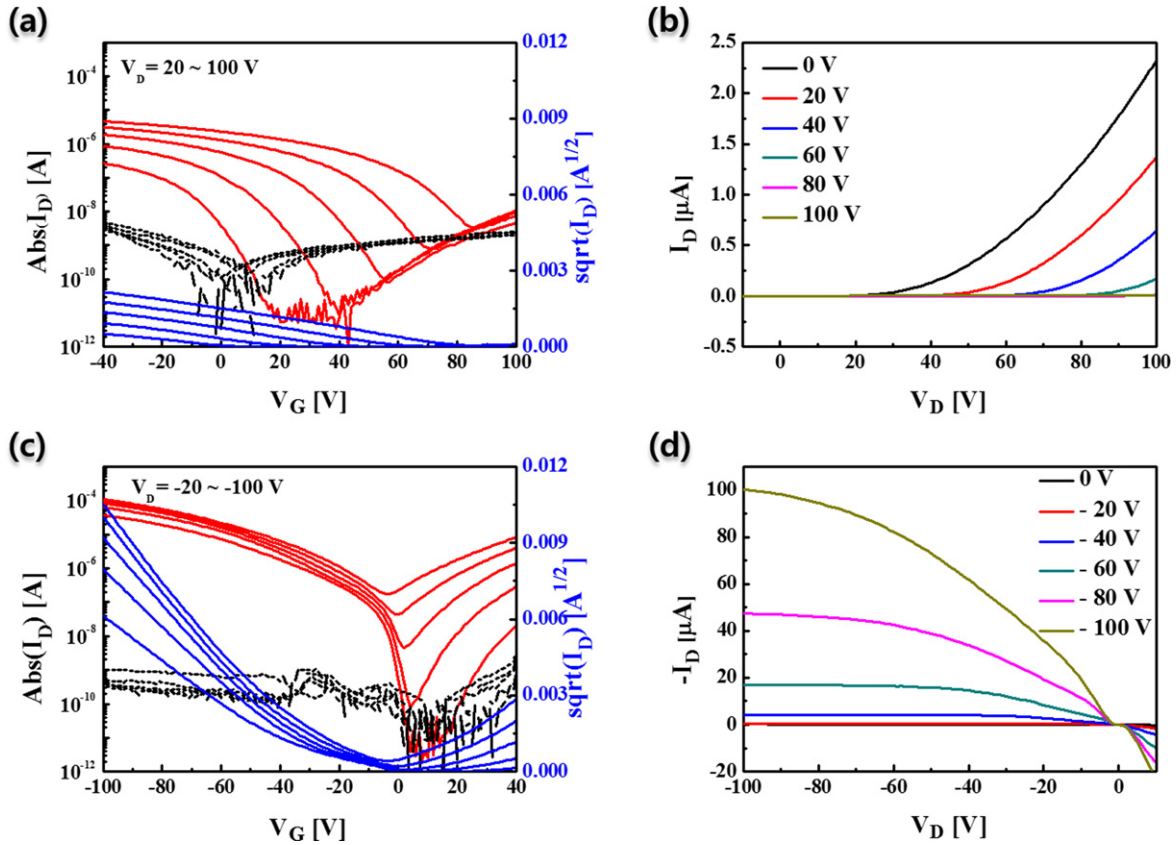

Figure 3. Transfer (I_D versus V_G) and output (I_D versus V_D) characteristics of ambipolar OFETs based on ROP Ag electrodes at the (a), (b) n-channel and (c), (d) p-channel regions.

not only the Ag nanoparticle ink but also the thermal annealing process at relatively high temperatures [28]. These silver oxides result in the ROP-Ag electrodes displaying p-type semiconducting properties and more effective hole injection into the channel (than electron injection) [25]. Figure 5(d) shows a peak at ~724 eV corresponding to the Cs 3d core levels. As can be observed in the scanning electron microscope (SEM) images shown in figures 5(e) and (f), the Cs salts are formed in the shape of nano-sized dots on the ROP-Ag electrode. These peak positions and surface images of the electrodes are consistent with the previously reported results in literature, and this means that the solution-processed Cs salts deposited by spin-coating on ROP-Ag do not consist of metallic Cs or Cs-suboxides; rather they consist of pristine salts [15].

We measured the work function (Φ) of the metal electrodes using UPS for the evaluation of the change in the energy barrier. The Φ values were calculated from the following equation: $\Phi = h\nu - W_e$, where $h\nu$ is the incident UV light containing 21.22 eV photons (He I line) and the width of the energy of the emitted electrons (W_e) was obtained from the onset of the secondary electrons at the Fermi edge. As mentioned above, the Φ of the ROP Ag electrodes cured at 250 °C was approximately −4.96 eV and PDPP-TAT had HOMO and LUMO levels of 5.39 eV and 3.89 eV, respectively. The results showed that the Φ of the ROP Ag electrodes changed from −4.96 to −4.5 eV when Cs_2CO_3 was spin-coated. This means that the energy barrier for the electron injection decreased, but that for the hole injection increased. We also confirmed the UPS spectra at the interface between Cs_2CO_3 and the semiconductor. This was achieved by spin-coating the Cs_2CO_3 and PDPP-TAT on ITO (indium tin oxide) coated-glass substrates. The Fermi level of PDPP-TAT was shifted towards the LUMO level, after the deposition of Cs_2CO_3 by spin-coating. Therefore, the effects of the deposition of Cs_2CO_3 layers are the n-type doping of PDPP-TAT and the decrease in the work function of the ROP Ag electrodes. Figure 6(b) shows the morphology of the semiconductor before and after the spin-coating of Cs_2CO_3 is characterized using AFM. After the spin-coated Cs_2CO_3 was randomly formed in the shape of nano-sized dots on PDPP-TAT, the root mean square (rms) roughness of the surface increased from 1.86 to 2.75 nm. However, there are no considerable changes in morphology at the surface of the PDPP-TAT after the deposition of Cs_2CO_3. It is proved that the variation in the electrical characteristics of the transistor is not caused by morphological modification of the active layer. These results indicate that the mobility of the n-channel operation increased, but that of the p-channel operation decreased because of the electronic changes caused by the deposition of Cs_2CO_3 between the semiconductors and the ROP Ag electrodes. In a previous work, Kim *et al* demonstrated the excellent electrical switching characteristics of flexible OFETs fabricated using an ROP Ag nanoparticle

Table 1. Fundamental parameters of ambipolar OFETs based on ROP Ag electrodes before and after deposition of Cs_2CO_3 on these electrodes. The devices have a 20 μm channel length, 1 mm width, and 2.17 nF cm^{-2} capacitance per unit area of the gate insulator.

	P-channel				N-channel			
Charge injection layer	μ_{sat} (cm^2 V^{-1} s^{-1})	V_T (V)	I_{on}/I_{off}	S (V decade^{-1})	μ_{sat} (cm^2 V^{-1} s^{-1})	V_T (V)	I_{on}/I_{off}	S (V decade^{-1})
None	0.35 (±0.022)	−32.3 (±2.55)	~10^4	−13.0 (±1.89)	0.0084 (±0.000 27)	56.1 (±3.01)	~10^2	27.2 (±4.45)
Cs_2CO_3	0.26 (±0.038)	−66.3 (±4.41)	~10^2	−20.8 (±3.27)	0.027 (±0.0015)	26.1 (±3.15)	~10^4	12.9 (±2.02)

electrode and a p-channel polymeric semiconductor on a polyimide substrate [25]. Compared to this device, our device has a comparable mobility for the p-channel operation, as well as significantly improved mobility for the n-channel operation as a result of using the low-band gap co-polymer and Cs_2CO_3. Furthermore, we can easily fabricate the complementary inverter with this low-band gap co-polymer and ROP Ag electrodes.

We demonstrated a complementary inverter with a donor–acceptor copolymer and ROP electrodes. An inverter whose electrodes were fabricated using the ROP method (figure 7(a)) is composed of two connected transistors (figure 7(b)). For the symmetry of the voltage transfer characteristics, the electrodes (channel length = 20 μm) have a width of 1 mm on the left and 10 mm on the right as shown in figure 7(a). These two transistors in the complementary inverter have a common gate with an input voltage of V_{in}, and a common drain with an output voltage of V_{out}. Out of the remaining two electrodes, the one on the left was biased at the supply voltage (V_{DD}); this region is the p-channel transistor, which is called the pull-up device in the complementary inverter. The other electrode on the right was biased to ground; this region is the n-channel transistor, which is called the pull-down device. If V_{in} is close to 0 V (i.e., V_{in} is low), the pull-up device (p-channel transistor) is in the on-state and the pull-down device (n-channel transistor) is in the off-state. This means that the output signal V_{out} is driven to the supply voltage. On the contrary, if V_{in} is close to V_{DD}, the state of each transistor is reversed and V_{out} is close to 0 V. When V_{in} is almost half of V_{DD}, the inverter exhibits switching characteristics.

Figures 7(c) and (e) show the voltage transfer characteristics of a complementary inverter based on ROP Ag electrodes with positive supply voltages; it has similar characteristics similar to those noted previously. It can be observed in figure 7(b) that V_{out}, which is driven to V_{DD}, shows excellent voltage characteristic aspects similar to those of an ideal complementary inverter with low V_{in}, because of the effective hole transport in the p-channel transistor. On the other hand, the inverter exhibited inferior device performance at high V_{in}. This was attributed to the poor device characteristics of the n-channel transistors, resulting from inferior electron transport. Although the channel of the n-channel transistor is ten times as wide as that of the p-channel transistor, the current of the pull-down device was not enough to drive V_{out} to ground.

The voltage transfer characteristics can also be significantly improved by the deposition of Cs_2CO_3 as an electron injection layer, as in the n-channel ambipolar OFETs studied previously. Cs_2CO_3 can be selectively deposited on the n-channel transistors of the complementary inverters by thermal evaporation with a shadow mask. Because of the selective deposition of Cs_2CO_3 on the n-channel region, the voltage transfer characteristics of the complementary inverter are similar to those of the non-Cs-processed ones when V_{in} is low. However, when V_{in} is high, the complementary inverter based on ROP Ag electrodes show highly enhanced voltage transfer characteristic curves because of the deposited film, which is largely composed of CsO_2 resulting from the decomposition of Cs_2CO_3 [18]. Figure 7(e) shows the modified voltage transfer characteristic curves, which exhibit excellent behavior that is similar to that of an ideal complementary inverter, and an improved gain parameter, because of the enhanced electron transport. Figures 7(d) and (f) show the gain parameter at each supplied voltage and the change in the inverting voltage (V_{inv}). Figure 7(d) shows the output voltage gains of the inverters based on the ROP Ag electrodes before the deposition of Cs_2CO_3. The maximum gains are approximately 4 at V_{DD} = 40 V, 7 at V_{DD} = 60 V, 9 at V_{DD} = 80 V, and 11 at V_{DD} = 100 V. Additionally, the inverters exhibited unstable gain values at high V_{in} because of the inferior electron transport in the n-channel transistors. As can be observed in figure 7(f), the inverters show greatly improved gain parameters after the deposition of Cs_2CO_3. The maximum gains are approximately 9 at V_{DD} = 40 V, 8 at V_{DD} = = 60 V, 11 at V_{DD} = 80 V, and 11 at V_{DD} = 100 V. In addition, V_{inv} shifted to ~5 V at V_{DD} = 40 V, ~4 V at V_{DD} = 60 V, ~7 V at V_{DD} = 80 V, and ~10 V at V_{DD} = 100 V approaching 1/2 V. This was attributed to the enhanced μ_{sat} of the n-channel transistors. The maximum gain and the inverting voltage for each supplied voltage are summarized in table 2.

A mechanical bending test of the ambipolar OFETs based on ROP Ag electrodes was performed to determine if these devices show superior performances without degradation of their electrical characteristics for flexible device applications. For the test, the device was attached to metal bending substrates with different radii varying from 100 to 10 mm. We observed the variation of μ_{sat}, which is an important parameter in the electrical properties of both the OFETs and the complementary inverter, as a function of the applied tensile strains ranging from 0.05% to 0.5% in the p-channel transistors (figure 8(a)). The inset in figure 8(a) shows the flexible device under the bending test. The tensile

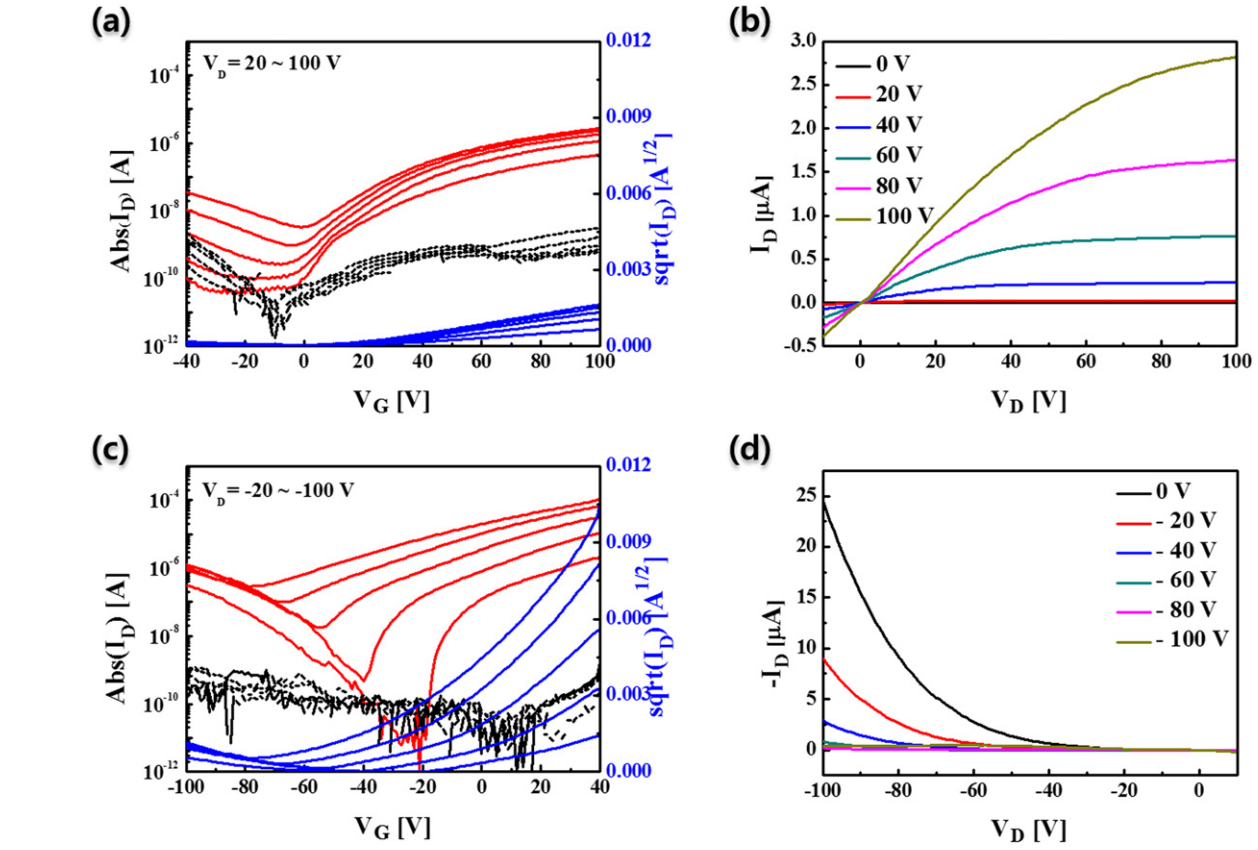

Figure 4. Transfer and output characteristics of ambipolar OFETs based on ROP Ag electrodes after spin-coating of Cs_2CO_3 at the (a), (b) n-channel and (c), (d) p-channel region.

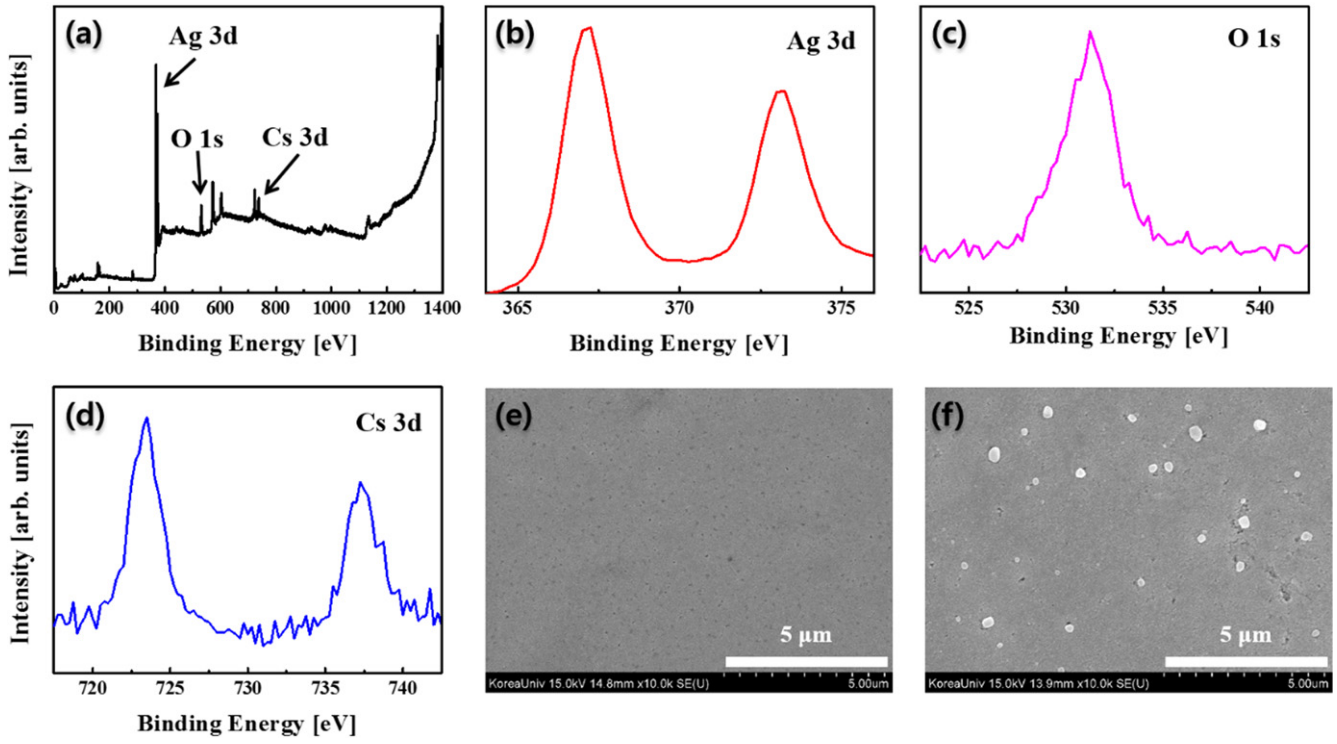

Figure 5. (a) X-ray photoelectron spectroscopy (XPS) spectra of the surface of Cs-processed ROP Ag. XPS spectra of (b) Ag 3d peak and (c) O 1s peak and (d) Cs 3d peak. Scanning electron microscopy (SEM) images of the surface of the ROP Ag electrodes (e) before and (f) after the deposition of Cs_2CO_3 by spin-coating.

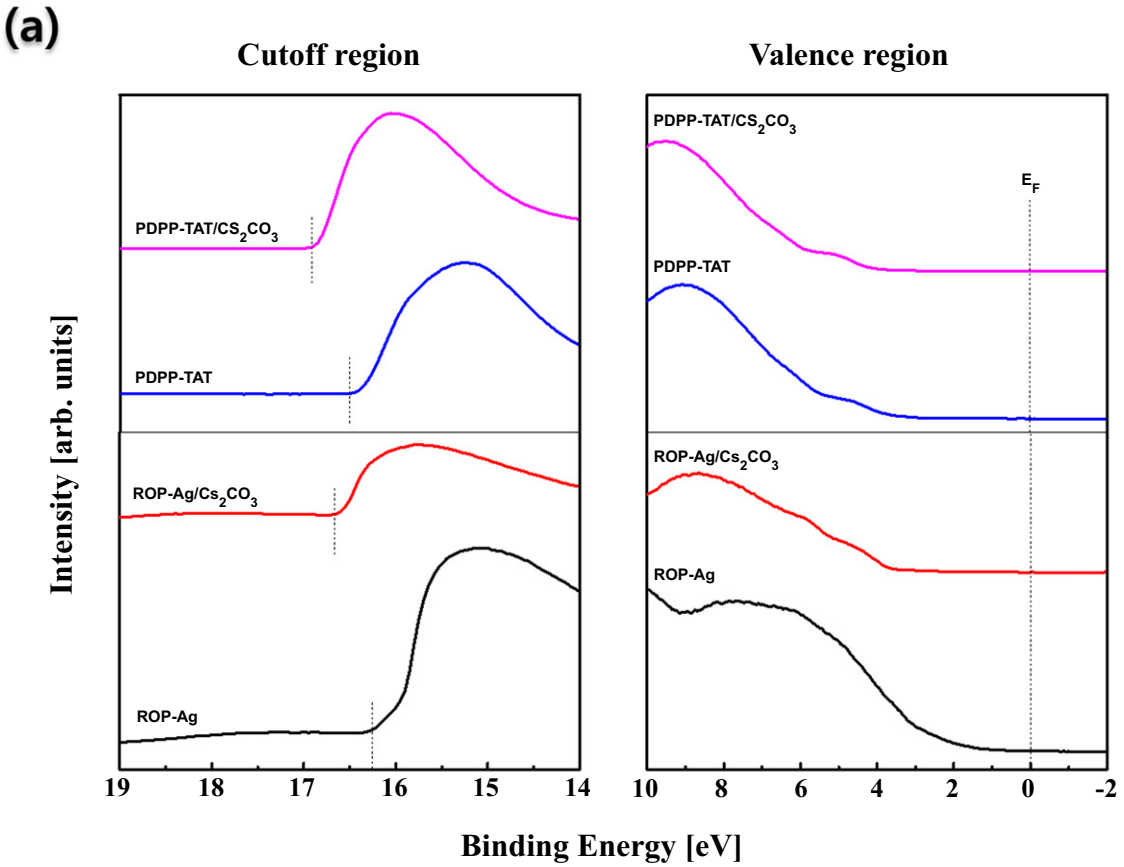

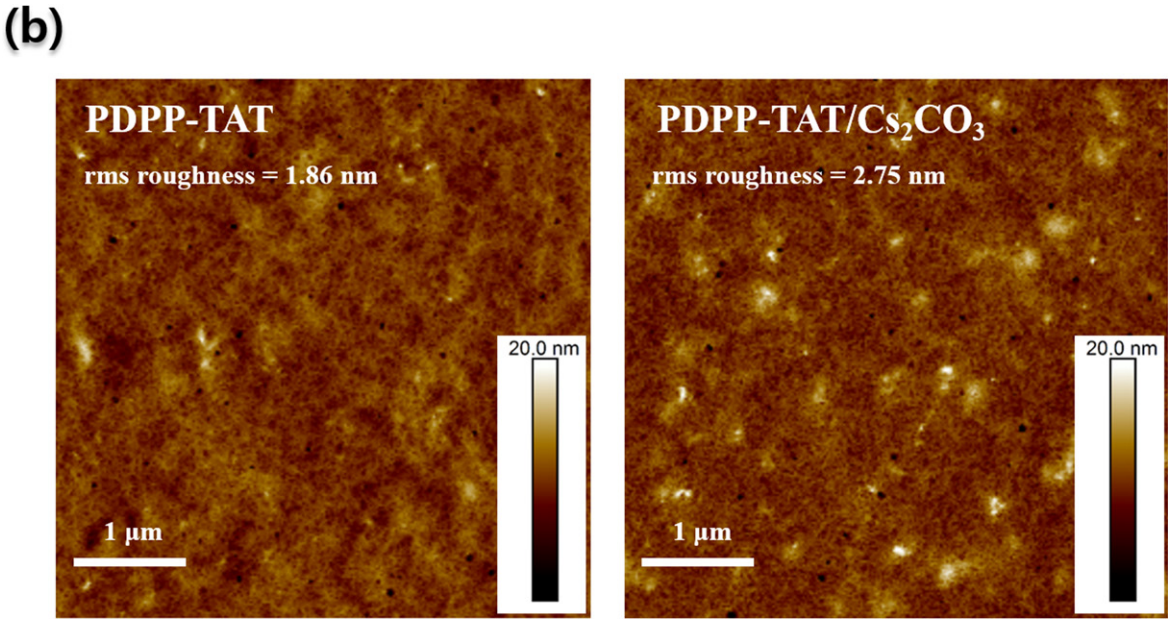

Figure 6. (a) Ultraviolet photoelectron spectroscopy (UPS) spectra of independent films of ROP Ag, ROP Ag/Cs_2CO_3, PDPP-TAT and PDPP-TAT/Cs_2CO_3. (b) AFM topographic images of PDPP-TAT and PDPP-TAT/Cs_2CO_3.

strain was calculated by

$$\text{Strain}\ (\%) = \frac{1}{[(2R/\Delta R)\ +\ 1]} \times\ 100, \qquad (4)$$

where R is the fixture radius, and ΔR is the thickness of the bent object containing the polyimide substrate (100 μm), Ag electrode (450 nm), PDPP-TAT semiconductor (80 nm), PMMA dielectric (1.8 μm), and Al gate (100 nm). In addition, the p-channel transfer characteristics of the ambipolar OFETs exhibited stable operation for bending radii ranging from 100 to 10 mm (figure 8(b)). A mechanical bending test of the n-channel transistors based on ROP Ag electrodes was also

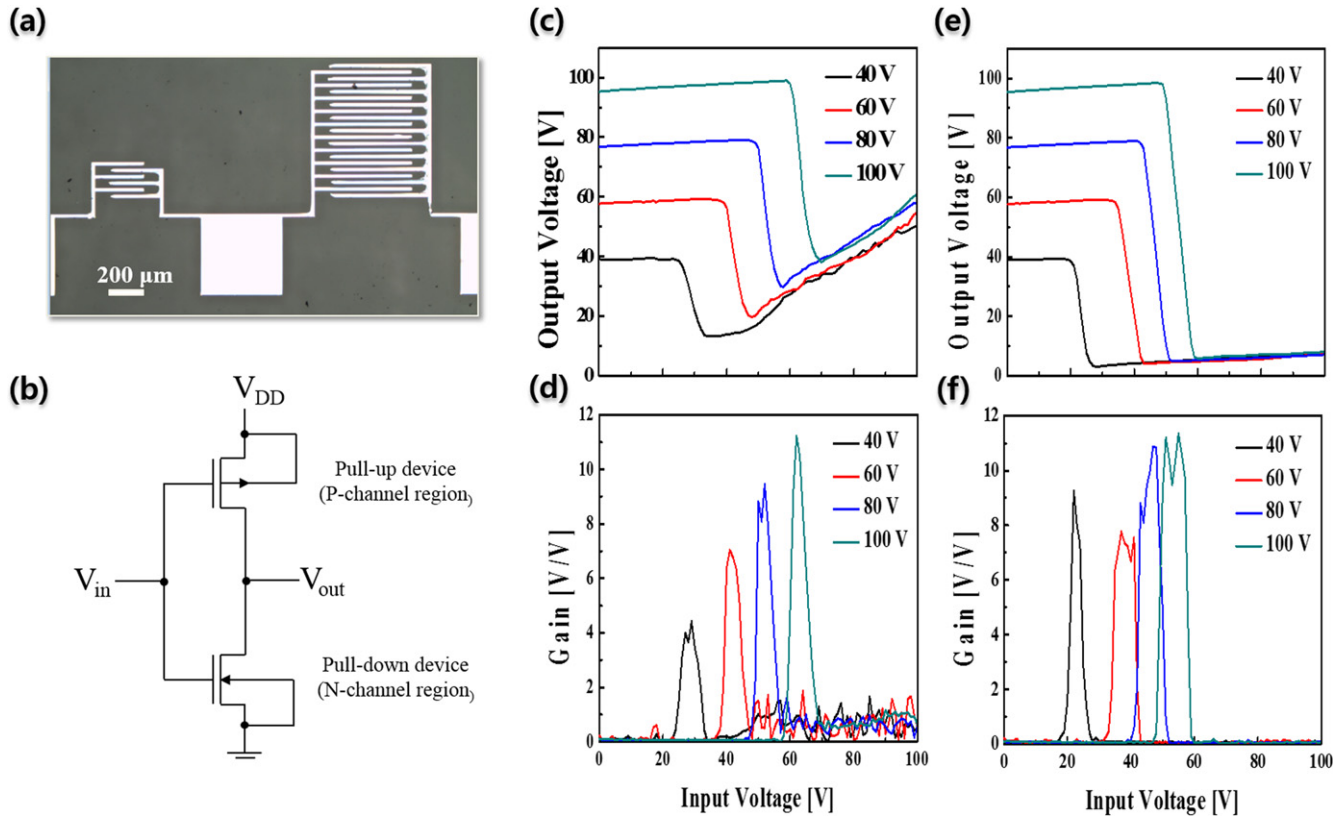

Figure 7. (a) Optical image of ROP electrodes for complementary inverter. (b) Circuit diagram of the complementary inverter. (c) Voltage transfer characteristics and (d) output voltage gains of the complementary inverter based on ROP Ag electrodes for different supply voltages. (e) Voltage transfer characteristics and (f) output voltage gains of the inverters after deposition of Cs_2CO_3 via thermal evaporation on the n-channel region.

Table 2. Maximum gain and inverting voltage of the complementary inverter based on ROP Ag electrodes at different supply voltage.

	Maximum gain (V/V)				Inverting voltage (V)			
Charge injection layer	40 V	60 V	80 V	100 V	40 V	60 V	80 V	100 V
None	4.4214	7.0428	9.4652	11.2271	28	42	53	64
Cs_2CO_3	9.2720	7.7724	10.8842	11.3706	23	38	46	54

evaluated after the deposition of Cs_2CO_3 by spin-coating at the interface between the semiconductors and electrodes. Figure 8(c) shows the variations in μ_{sat} as a function of the applied tensile strain, which was calculated using equation (4). Because the Cs_2CO_3 layer was deposited in the form of pristine salts, it did not affect the calculation of the tensile strain. In addition, during the bending test, the ambipolar OFETs exhibited n-channel transfer characteristics for tensile strains ranging from 0.05% to 0.5% without noticeable change (figure 8(d)). The results indicate that our flexible device exhibits stable properties under the various bending radii ranging from 100 mm to 10 mm. In a previous work, Yun *et al* fabricated OFETs with a PDPP-TAT and Al layer as the source-drain electrodes on a Si-on-insulator wafer [29]. This device exhibited a higher electron mobility and hole mobility than that of our device. However, in their method, as the device is formed on a Si wafer, it is impossible to apply this device to flexible electronic devices. Because the mechanical stability of flexible devices is an essential characteristics, our OFETs can be used in flexible electronic devices.

4. Conclusions

Flexible ambipolar OFETs and complementary inverters based on roll-to-plate ROP methods were fabricated using low-bandgap co-polymers (PDPP-TAT). The saturation mobility values, which are optimized by controlling the charge injection between the semiconductors and the electrodes, are $0.35\ cm^2\ V^{-1}\ s^{-1}$ (p-channel) and $0.027\ cm^2\ V^{-1}\ s^{-1}$ (n-channel). A complementary inverter was fabricated with roll-to-plate ROP Ag electrodes and it exhibited improved electrical characteristics, which are similar to the ideal characteristics, as a result of the insertion of Cs_2CO_3 onto the n-channel region via thermal evaporation. Finally, excellent mechanical stability is demonstrated for

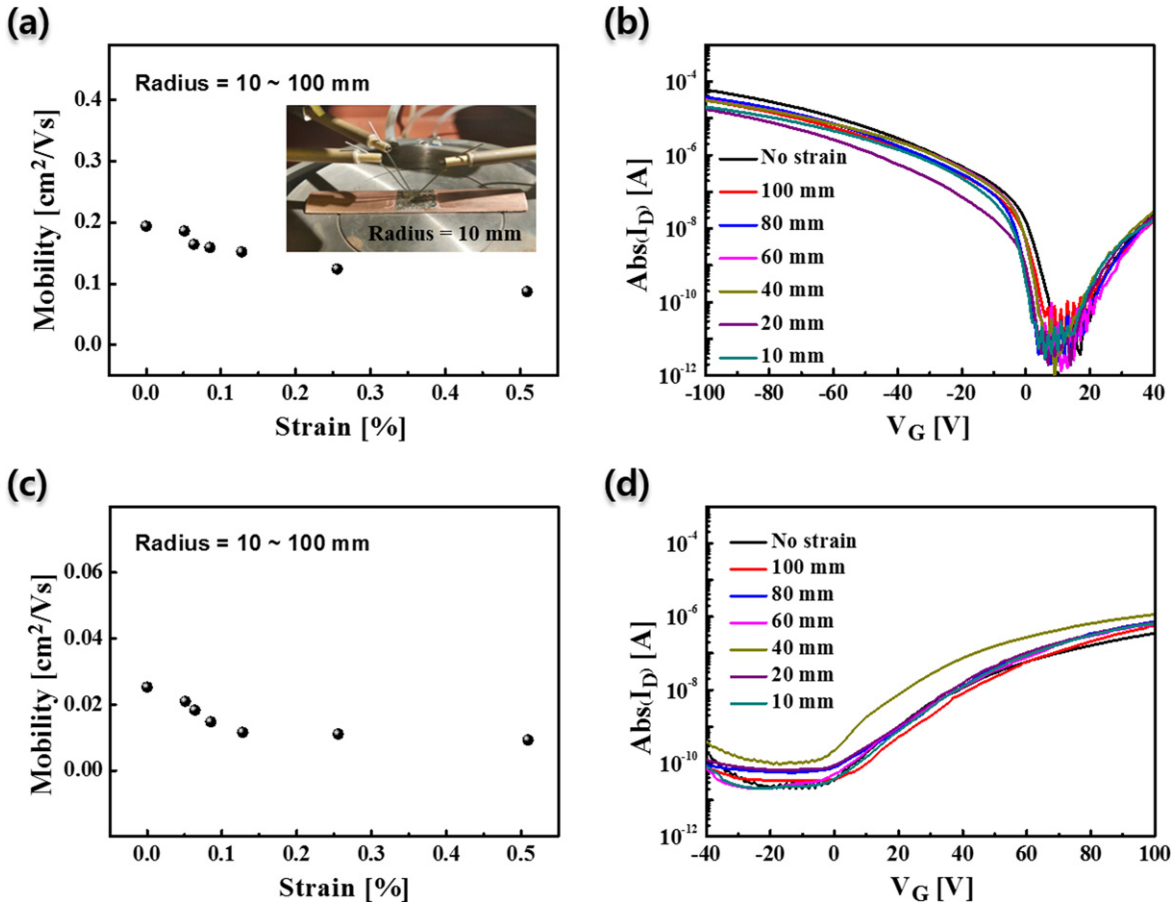

Figure 8. Mechanical bending test results. Variation in μ_{sat} of flexible ambipolar OFETs for (a) p-channel and (c) n-channel operation as a function of applied tensile strain. Inset shows the device on the bending substrate. Transfer characteristics for (b) p-channel and (d) n-channel operation of the same device.

applied tensile strains of up to 0.5%. Therefore, these results confirm that our devices have great potential for use in low-cost printed and flexible integrated circuits over a large area.

Acknowledgments

This work was partly supported by Institute for Information and Communications Technology Promotion (IITP) grant funded by the Korea government (MSIP) (B0101-16-0133, the core technology development of light and space adaptable energy-saving I/O platform for future advertising service) and Korea Evaluation Institute of Industrial Technology (KEIT) grant funded by the Korea government (MOTIE) (10048317, Development of red and blue OLEDs with external quantum efficiency over 20% using delayed fluorescent materials). The work was also supported by the KSSRC program (Stretchable Multi Sensor for Wearable IoT Device).

References

[1] Forrest S R 2004 The path to ubiquitous and low-cost organic electronic appliances on plastic *Nature* **428** 911–8

[2] Gelinck G, Heremans P, Nomoto K and Anthopoulos T D 2010 Organic transistors in optical displays and microelectronic applications *Adv. Mater.* **22** 3778–98

[3] Baeg K J, Khim D, Kim J, Yang B D, Kang M, Jung S W, You I K, Kim D Y and Noh Y Y 2012 High-performance top-gated organic field-effect transistor memory using electrets for monolithic printed flexible NAND flash memory *Adv. Funct. Mater.* **22** 2915–26

[4] Crone B, Dodabalapur A, Gelperin A, Torsi L, Katz H E, Lovinger A J and Bao Z 2001 Electronic sensing of vapors with organic transistors *Appl. Phys. Lett.* **78** 2229–31

[5] Zaumseil J and Sirringhaus H 2007 Electron and ambipolar transport in organic field-effect transistors *Chem. Rev.* **107** 1296–323

[6] Schon J H, Meng H and Bao Z 2000 Ambipolar pentacene field-effect transistors and inverters *Science* **287** 1022–3

[7] Meijer E J, de Leeuw D M, Setayesh S, van Veenendaal E, Huisman B H, Blom P W M, Hummelen J C, Scherf U, Kadam J and Klapwijk T M 2003 Solution-processed ambipolar organic field-effect transistors and inverters *Nat. Mater.* **2** 834

[8] Muccini M 2006 A bright future for organic field-effect transistors *Nat. Mater.* **5** 605–13

[9] Dinelli F, Capelli R, Loi M A, Murgia M, Muccini M, Facchetti A and Marks T J 2006 High-mobility ambipolar transport in organic light-emitting transistors *Adv. Mater.* **18** 1416

[10] Capelli R, Toffanin S, Generali G, Usta H, Facchetti A and Muccini M 2010 Organic light-emitting transistors with an

efficiency that outperforms the equivalent light-emitting diodes *Nat. Mater.* **9** 496–503
[11] Colladet K *et al* 2007 Low band gap donor–acceptor conjugated polymers toward organic solar cells applications *Macromolecules* **40** 65–72
[12] Ashraf R S *et al* 2011 Silaindacenodithiophene semiconducting polymers for efficient solar cells and high-mobility ambipolar transistors *Chem. Mater.* **23** 768–70
[13] Loser S, Bruns C J, Miyauchi H, Ortiz R P, Facchetti A, Stupp S I and Marks T J 2011 A naphthodithiophene-diketopyrrolopyrrole donor molecule for efficient solution-processed solar cells *J. Am. Chem. Soc.* **133** 8142–5
[14] Zhao Y, Guo Y L and Liu Y Q 2013 25th anniversary article: recent advances in n-type and ambipolar organic field-effect transistors *Adv. Mater.* **25** 5372–91
[15] Baeg K J, Kim J, Khim D, Caironi M, Kim D Y, You I K, Quinn J R, Facchetti A and Noh Y Y 2011 Charge injection engineering of ambipolar field-effect transistors for high-performance organic complementary circuits *Acs Appl. Mater. Interfaces* **3** 3205–14
[16] Liao H H, Chen L M, Xu Z, Li G and Yang Y 2008 Highly efficient inverted polymer solar cell by low temperature annealing of Cs(2)CO(3) interlayer *Appl. Phys. Lett.* **92** 173303
[17] Zhang X W, Xu J W, Xu H R, Lin H P, Li J, Jiang X Y and Zhang Z L 2013 Improving electron injection and microcavity effect for constructing highly efficient inverted top-emitting organic light-emitting diode *Opt. Laser Technol.* **45** 181–4
[18] Huang J S, Xu Z and Yang Y 2007 Low-work-function surface formed by solution-processed and thermally deposited nanoscale layers of cesium carbonate *Adv. Funct. Mater.* **17** 1966–73
[19] Yan H, Chen Z H, Zheng Y, Newman C, Quinn J R, Dotz F, Kastler M and Facchetti A 2009 A high-mobility electron-transporting polymer for printed transistors *Nature* **457** 679–U1
[20] Zielke D, Hubler A C, Hahn U, Brandt N, Bartzsch M, Fugmann U, Fischer T, Veres J and Ogier S 2005 Polymer-based organic field-effect transistor using offset printed source/drain structures *Appl. Phys. Lett.* **87** 123508
[21] Noh Y Y, Zhao N, Caironi M and Sirringhaus H 2008 Downscaling of self-aligned, all-printed polymer thin-film transistors (vol 2, pg 784, 2007) *Nat. Nanotechnol.* **3** 58
[22] Pardo D A, Jabbour G E and Peyghambarian N 2000 Application of screen printing in the fabrication of organic light-emitting devices *Adv. Mater.* **12** 1249–52
[23] Makela T, Jussila S, Kosonen H, Backlund T G, Sandberg H G O and Stubb H 2005 Utilizing roll-to-roll techniques for manufacturing source-drain electrodes for all-polymer transistors *Synth. Met.* **153** 285–8
[24] Moon T H, Nam S H, Kim N K, Kook Y H, Jung Y K, Chang Y G, Yoo S S, Kim C D, Kang I and Chung I J 2009 P-185L: late-news poster: direct patterning of metal electrodes for TFT-LCD fabrication *SID Int. Symp. Dig. Tech. Pap.* **40** 1348
[25] Kim M, Ha H J, Yun H J, You I K, Baeg K J, Kim Y H and Ju B K 2014 Flexible organic phototransistors based on a combination of printing methods *Org. Electron.* **15** 2677–84
[26] Gelinck G H *et al* 2004 Flexible active-matrix displays and shift registers based on solution-processed organic transistors *Nat. Mater.* **3** 106–10
[27] Merlo J A, Newman C R, Gerlach C P, Kelley T W, Muyres D V, Fritz S E, Toney M F and Frisbie C D 2005 p-channel organic semiconductors based on hybrid acene-thiophene molecules for thin-film transistor applications *J. Am. Chem. Soc.* **127** 3997–4009
[28] Kim M, You I K, Han H, Jung S W, Kim T Y, Ju B K and Koo J B 2011 Organic thin-film transistors with short channel length fabricated by reverse offset printing *Electrochem. Solid State Lett.* **14** H333–6
[29] Yun H J, Choi H H, Kwon S K, Kim Y H and Cho K 2014 Conformation-insensitive ambipolar charge transport in a diketopyrrolopyrrole-based co-polymer containing acetylene linkages *Chem. Mater.* **26** 3928–37
[30] Jin S H, Yu J S, Lee C A, Kim J W, Park B G and Lee J D 2004 Pentacene OTFTs with PVA gate insulators on a flexible substrate *J. Korean Phys. Soc.* **44** 181–4
[31] Baeg K J, Khim D, Jung S W, Koo J B, You I K, Nah Y C, Kim D Y and Noh Y Y 2011 Polymer dielectrics and orthogonal solvent effects for high-performance inkjet-printed top-gated p-channel polymer field-effect transistors *ETRI J.* **33** 887–96